Forestry: An International Journal of Forest Research, 2026, 99(2), cpag006
https://doi.org/10.1093/forestry/cpag006
Published: 15 February 2026
Original Article

Institute of Chartered Foresters
OXFORD

The application of intra-canopy photogrammetry for assessing crown health attributes in sugar maple (*Acer saccharum* Marsh.)

Lukas G. Olson[1,*], Nicholas C. Coops[1], Guillaume Moreau[2], Richard C. Hamelin[3], Alexis Achim[2]

[1]Department of Forest Resources Management, Faculty of Forestry & Environmental Stewardship, University of British Columbia, 2424 Main Mall, Vancouver, BC V6T 1Z4, Canada
[2]Département des Sciences du Bois et de la Forêt, Faculté de foresterie, de géographie et de géomatique, Université Laval, 2425 rue de la Terrasse, Québec, QC, G1V 0A6, Canada
[3]Department of Forest and Conservation Sciences, Faculty of Forestry & Environmental Stewardship, University of British Columbia, 2424 Main Mall, Vancouver, BC, V6T 1Z4, Canada

*Corresponding author. Department of Forest Resources Management, Faculty of Forestry & Environmental Stewardship, University of British Columbia, 2424 Main Mall, Vancouver, BC V6T 1Z4, Canada. E-mail: olson@student.ubc.ca

Abstract

The northern hardwood forests of Eastern Canada, particularly stands dominated by sugar maple (*Acer saccharum* Marsh.), are facing ongoing decline due to historical and contemporary environmental pressures. Traditional ground-based crown assessments for tree health are essential for management, but can be subjective, costly, and limited by their viewing perspective. While conventional remote sensing methods can effectively capture tree crown structure from above, and terrestrial approaches can capture the stems and crowns from beneath, occlusion by the dense crowns of mature sugar maples makes capturing reliable estimates challenging. We examine the potential of intra-canopy aerial drone-based photogrammetry, involving flights beneath, within, and above tree crowns, to generate detailed 3D point clouds of 29 sugar maple trees in Quebec, Canada. From these point clouds, we derived estimates of key structural attributes including diameter at breast height (DBH), tree height, and crown base height (CBH). We used ray-marching to quantify crown transparency across 162 viewing angles, forming a sphere around the crown, and compared predictions to ground-based visual estimates and health categories. Photogrammetric estimates had significant correlations with ground-measured attributes, including DBH ($r = 0.82$), tree height ($r = 0.55$), and CBH ($r = 0.73$ and 0.78 across two distinct definitions). Modeled crown transparency correlation was also significant when compared to ground-based visual assessments ($\rho = 0.54$), suggesting that intra-canopy drone-based photogrammetry can offer rapid and objective assessment of crown condition.

Keywords **tree health, deciduous, sugar maple, crown transparency, uncrewed, aerial vehicle, photogrammetry**

Introduction

The northern hardwood Forests of Eastern Canada and the Northeastern United States provide significant economic, cultural, and biodiversity ecosystem services. One of the most valuable species within these forests, the sugar maple (*Acer saccharum* Marsh.), contributes a substantial portion of the regional forest productivity, yields valuable economic products including maple syrup and timber, and provides critical habitat for wildlife. Since the 1980s, however, the sugar maple has faced considerable decline, driven by factors including climate change and suboptimal management decisions (Bishop et al. 2015, Cleavitt et al. 2018). Historic disturbances and processes, like acid deposition from the eastern North American manufacturing industry, poor stand management, and agricultural land use, have led to soil acidification and reduced soil nutrient levels across large portions of the sugar maple range, which negatively impact winter hardiness and photosynthetic efficiency (Caputo et al. 2016). Simultaneously, warming winter temperatures increase forest pest survival and reduce snowpack, exacerbating summer drought conditions, and exposing the shallow roots of sugar maple to freezing temperatures (Oswald et al. 2018).

While legislative efforts in Canada and the United States (e.g. the 1985 Eastern Canada Acid Rain Program, the 1990 U.S. Clean Air Act amendments, and the 1991 Canada-United States Air Quality Agreement) have reduced regional industrial emissions (Gbondo-Tugbawa et al. 2002), challenges remain in managing these stands because of lasting nutrient deficiencies and forest decline. To improve ecosystem health and function, while maintaining an economically suitable harvest, Canadian northern hardwood stands are managed at the individual tree level by specially trained foresters using selection cutting. Trees with poor growth and a high probability of mortality

Handling editor: Fabian Fassnacht
Received 11 September 2025. **revised** 24 December 2025. **accepted** 18 January 2026

(low vigor) are prioritized for harvest, while trees with good growth and a low probability of mortality (high vigor) are retained for the next harvest cycle (Pothier et al. 2013, Moreau et al. 2023a).

Various systems have been developed to quantify tree vigor and guide tree marking decisions, of which many rely on extensive and complex ground-based observations made across hundreds of stem and crown defects. Suggestions to simplify these systems have been proposed, including by (Moreau et al. 2023a, 2023b), who argued that because the photosynthetic capacity of a tree is dependent on the size and condition of its crown, with healthy tree crowns heavily associated with greater growth rates, health, and survival (Zarnoch et al. 2004, Tominaga et al. 2008), crown condition should be used as the primary indicator of tree vigor. These simplified approaches are supported by strong precedent, as many forest health monitoring programs considering crown condition have already been established for deciduous species, including the International Co-operative Programme on Assessment and Monitoring of Air Pollution Effects on Forests (ICP forests) in Europe (de Vries et al. 2003) and the Enhanced Forest Inventory and Analysis (FIA) program in the United States (Randolph et al. 2010, Randolph 2013).

Crown condition can be visually assessed through a combination of attributes visible from the ground, including crown dieback, defoliation, discoloration, and foliage abundance (assessed through crown density and transparency). Although individual systems and definitions vary across jurisdictions, their assessments are often similar in practice. Crown dieback can be defined as the percentage of the live crown where leaf and fine twig mortality has occurred. Crown density is the amount of crown biomass that blocks light visibility through the live crown outline. Crown transparency, or foliage transparency, is the inverse of crown density and is the proportion of sky or background visible through the live crown (Schomaker et al. 2007). Crown discoloration includes any symptom that may cause individual leaves to not appear green (e.g. chlorosis). Among these indicators, recent work in the northern hardwood forests have found that crown density (transparency), followed by crown dieback, are the best attributes for predicting both the growth potential and survival rates in sugar maple and yellow birch (*Betula alleghaniensis* Britt.) (Morin et al. 2015, Moreau et al. 2020b).

Although crown condition is less complex to assess than the current tree marking systems, challenges remain. Despite being quick to observe and widely applied, visual crown assessments are inherently qualitative and subjective, and can be highly biased (Ferretti 1997, Frampton et al. 2002). Perceptual differences among ground observers can introduce significant measurement bias (Redfern and Boswell 2004), with further variability introduced by differences in training and field methodology, tree age, crown size, and drought conditions (Metzger and Oren 2001; Cherubini et al. 2021). This suggests that while ground-based measurements are sufficient for many tree marking purposes, comparisons and modeling across stands and uncalibrated ground observers are problematic. Further, the calibration process can be expensive, requiring extensive training and coordination between individual markers, potentially across regions. As a result, there are growing demands across natural and urban forest environments for methods that can quantitatively assess tree crown attributes, serving as a comparative standard to facilitate training and baseline calibration, and which can be applied to help improve the objectivity of conventional assessment standards.

As an established, albeit potentially subjective, metric, foliage abundance has been adopted as a primary crown condition indicator for its strong link to overall tree health (Randolph 2006). Previous studies have explored its properties, sources of error, and observational limitations to develop more objective and accurate estimation methods. Proposed remote sensing approaches have largely focused on terrestrial photographs taken below or to the side of the crown. One early model, Crown Condition (CROCO), quantitatively estimates crown density in binary images by measuring the difference between a tree's visible foliage and its silhouette. While this approach faces challenges when canopies overlap in the images by >50% of the crown width or when facing restricted crown visibility, CROCO has been shown to be more consistent and reliable than conventional observation-based assessments (Mizoue and Dobbertin 2003). More recent models have further developed these principles and decomposed foliage abundance into its visual elements, using ground-based binary crown images to identify soft and deep crown indentations and differentiate between micro and macro crown holes (Borianne et al. 2017).

Remote sensing technologies have also been used to create accurate 3D models for forest health assessment and inventorying programs. These include light detection and ranging (lidar), an active technology, which emits and detects laser pulses to create highly accurate spatialized measurements, and digital photogrammetry, a complementary passive technology that calculates depth information from pairs of overlapping images (Goodbody et al. 2019, Ecke et al. 2022, 2024). Lidar and photogrammetry surveys, taken from above or below the canopy, are becoming increasingly common for characterizing individual trees attributes, including the assessment of DBH, and branch structure (Miller et al. 2015, Giannetti et al. 2018), canopy penetration (Lee and Lucas 2007), the vertical arrangement of crown fuels (Arkin et al. 2021), insect defoliation (Goodbody et al. 2018), and crown volume (Zhu et al. 2021). However, challenges remain in capturing the inner portions of the crown in sugar maple because of the vertical complexity and occlusion found in high density stands, and high cost associated with TLS/ALS fusion.

Drones, commonly referred to as uncrewed aerial vehicles, have emerged as versatile platforms for collecting digital photogrammetric and lidar data. While conventionally flown above the forest canopy, they have also been demonstrated, under controlled forest environments, capable of flying beneath the canopy to estimate individual tree DBH (Chisholm et al. 2013; Chisholm et al. 2021; Zhang et al. 2022), and in urban contexts, able to capture imagery of individual tree branches and reconstruct digital models with strong measurement correlation ($r = 0.99$) against standard physical measurements (Roberts et al. 2018, Scher et al. 2019). Beyond branch structure under leaf-off conditions, Olson et al. (2025) investigated first-person view (FPV) video drones for the photogrammetric reconstruction of individual open-grown urban deciduous trees. They compared DBH, height, and crown spread with ground measurements across leaf-on and leaf-off conditions, and proposed ray-marching as a mechanistic approach to estimate crown transparency, arguing it as analogous to the principles of ground-based transparency assessments. Overall, they found strong correlation between photogrammetry and lidar for Height ($r = 0.93$, MAE = 1.13 m), and crown spread ($r = 0.89$, RMSE = 2.42 m), and between photogrammetry and ground-measurements for DBH ($r = 0.98$, MAE = 3.87 cm), and moderate correlation for transparency ($r = 0.66$, MAE = 16.67%).

Drone-based intra-canopy photogrammetry has demonstrated strong reconstruction fidelity with minimal distortion, low measurement error, and high correlations with ground-based measurements, highlighting the potential to facilitate objective and quantitative estimates of tree attributes. These estimates could be used as a

comparative standard for ground-based assessors but are limited by having been predominantly developed and evaluated across open-grown trees under urban forest conditions. It remains unclear whether the feasibility or performance of drone imagery for photogrammetry is sufficient in denser forest stands. Further, the application of photogrammetry under these conditions in natural environments faces several uncertainties, including fluctuations in lighting conditions, branch movement, and poor visual distinction between the foreground and background. This study aims to adapt the methodology of Olson et al. (2025) to more dense sugar maple stands, addressing several of these challenges most relevant to future sugar maple crown condition research and evaluation. In doing so, we investigate three key areas, including (i) whether the use of consumer-grade FPV drones within tree canopies can provide sufficient visual coverage for close-range photogrammetric reconstruction; (ii) how the agreement between tree-level attributes extracted through tree-level point cloud analysis and ground-assessed equivalents compares for structural attributes (DBH, height); and (iii), how ray-marched crown transparency estimates, as seen from different viewing positions, compare with ground-estimated values.

To do this, we first establish a method for intra-canopy drone-based photogrammetry in moderately dense northern hardwood stands to create complete, 3D colored point clouds of individual sugar maple trees. Second, we spatially compare the agreement and precision of key tree attributes, associated with sugar maple health, between ground-measured and point cloud-derived estimates. Third, we calibrate, decompose, and assess a ray-marching-based model using ground-based assessments to predict crown foliar transparency from these point clouds.

Materials and methods

Study region

Field measurements were taken across four nearby areas in a northern hardwood stand in the Centre-du-Québec region of Quebec, Canada (Fig. 2), composed of sugar maple and yellow birch, following selective cuts that occurred between 2018 and 2020. The treatment removed ∼30% of the initial basal area, resulting in residual stands of ∼200 stem/ha. This region experiences an annual precipitation of 1280 mm, with winter temperatures averaging −11°C and 270 mm of precipitation. Summertime temperatures reach an average of 17°C, with an average of 390 mm. Spring and autumn share similar precipitation patterns, with temperatures ranging from −5°C to 10°C (Environment and Climate Change Canada, 2025). The soils in this region are podzolic, with stony glacial till and granite gneiss as the parent material, originating from the Canadian Shield (Ouimet et al. 2013). Dominant tree species include sugar maple, red maple (*Acer rubrum* L.) and yellow birch, and an understory comprising eastern hemlock [*Tsuga canadensis* (L.) Carrière], American beech (*Fagus grandifolia* Ehrh.), Hobblebush (*Viburnum lantanoides* Michx.), and, less commonly, Witch-Hazel (*Hamamelis virginiana* L.). Twenty-nine sugar maple trees across the four plots were sampled in August 2024.

Distribution of study trees

Tree DBH was left-skewed, ranging from 16.10 cm to 46.20 cm, with a mean DBH of 25.69 cm and standard deviation of 6.92 cm (Fig. 1a). Tree heights had a wider distribution and right skew, ranging from 8.28 m to 23.73 m, with a mean ground-measured height of 14.21 m, and a standard deviation of 3.26 m (Fig. 1b).

Data collection

Ground-truth

For each tree, a trained field crew collected dendrometric and crown health data. DBH was measured to the nearest 0.1 cm at 1.3 m above ground level using a standard DBH tape. Tree height was measured using the tangent clinometer method, where an observer established a clear line of sight to each treetop. The horizontal distance to the tree (HD) was measured using a meter tape, and the angle to the crown top (θ) was measured using a clinometer. Total tree height was calculated using the formula height = (HD × tan(θ)) + He, where He is the observer's eye height (1.68 m). Finally, crown transparency, defined as the percentage of the skylight visible through the crown, was visually estimated in 5% increments from 5%–100% and calibrated using a USDA Forest Service crown rating card (Schomaker et al. 2007).

Drone image collection

Drone-based video acquisitions for photogrammetric measurements were taken under low-wind conditions, adopting the orbital methodology described by Olson et al. (2025). Video was acquired using two DJI Avata FPV drone systems (Shenzhen DJI Science and Technology Ltd.; Shenzhen, China) at a resolution of 3840 × 2160 pixels and framerate of 60 frames per second (FPS). The Avata platform was chosen for its small, compact design, market accessibility for practitioners, and image fidelity. Further, its integrated FPV piloting system and propeller ducts help improve flight safety, maneuverability under complex close-proximity flight paths, and impact resilience. To reduce oversaturation above and undersaturation below the canopy caused by lighting differences, and to preserve textural detail negatively impacted by motion blur, camera parameters (ISO and shutter speed) were optimized throughout the day for the available light by selecting the lowest ISO and shutter speed values where textural details were visible without needing to increase video brightness. The duration of each video capture was recorded.

To provide a reference in the scene for automated scaling and orientation, a 0.5 × 0.5 × 0.5 m^3 reference cube was created from five polyethylene terephthalate glycol (PETG) panels manufactured using fused deposition modeling, commonly referred to as '3D Printing', and placed in the scene near the target tree. Each panel was marked with a unique circular coded target, allowing it to be uniquely identified and paired with the panel on the opposing face (see Supplementary material). Similarly, to facilitate easier identification of each tree during processing and validate the scaling, a unique, numbered, circular-coded target was attached to the stem of each tree and recorded with the field measurements.

Each drone flight launched from a sheet of plywood placed within the stand near the target tree. First, video capture was initiated, and the drone faced and circled the reference cube. The drone was then maneuvered to face the target tree at an HD of ∼2 m, with an altitude of 0.5 m. Orbits then began around the tree at a speed between 1 and 2 m/s, maintaining consistent altitude and radial distance, and with a target frame overlap of at least 50% (Gatziolis et al. 2015). After each orbit, drone altitude was increased while maintaining 50% vertical overlap, and the maneuver was repeated. When the drone reached the crown base, radial distance to the stem was increased. Whenever branches obstructed a safe orbit, the flight path was adjusted to face

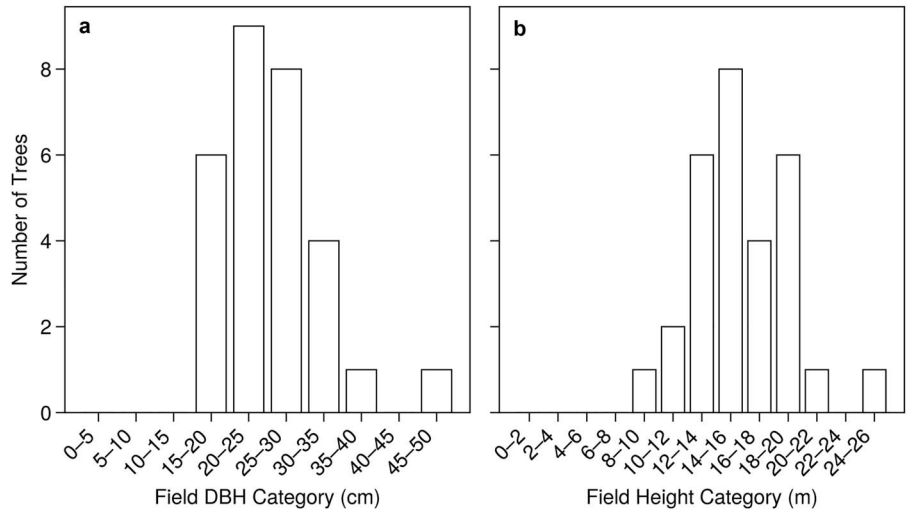

Figure 1 Distribution of tree size for the 29 trees sampled in this study. (a) Field-measured diameter at breast-height (DBH) grouped into 5 cm increments vs. number of trees. (b) Field-measured height grouped into 2 m increments vs. number of trees.

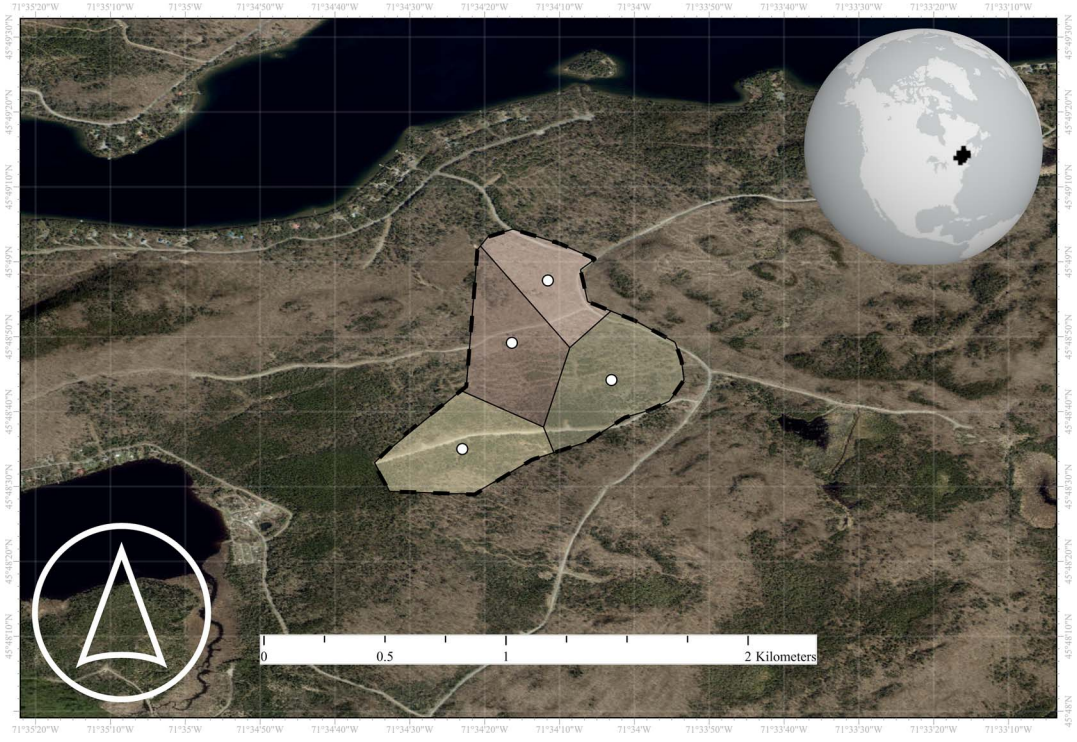

Figure 2 Study region within the Centre-du-Québec administrative region, Quebec, Canada. Each white dot represents the center of an area. The total survey area (~0.49 km^2) was conducted from the roadsides and on foot to locate sample trees. Basemap source: World Imagery (Esri 2024). Basemap data: Esri, NASA, NGA, USGS, FEMA, ARCM, Maxar.

and follow each branch at a 45-degree angle from the bole to the outside of the crown. If surrounding vegetation continued to obstruct the orbit, this flight pattern was then reversed, and the drone approached the obstruction from the opposite direction before continuing. Due to the challenges associated with navigating around moving branches in the forest canopy environment, when fine branches and gaps smaller than the drone were reached near the top of the crown, the drone moved to the outside of the crown and the orbit was continued. When a fork was reached in the stem, the orbit radius was increased to encapsulate both parts.

Processing approach

Photogrammetric reconstruction

To generate the 3D point clouds of the sugar maples from the recorded drone imagery, we extended the automated photogrammetry reconstruction workflow outlined in Olson et al. (2025). The original workflow can be summarized as five key steps: frame extraction, image registration, sparse cloud filtering, point cloud generation, and point cloud registration. In this study, because many images contained overly dark or bright regions from changes in lighting

Table 1 Processing parameters for the photogrammetric reconstruction process.

Parameter	Value
FPS	3 FPS
Feature matching resolution	3840 × 2160 px
Generic pre-selection	Enabled
Stationary point filtering	Disabled
Reference preselection	Disabled
Tie-point limit	60 K
Key-point limit	No limit
Camera alignment	Adaptive fitting
Reconstruction uncertainty threshold	100 units
Reprojection error threshold	1 px
Projection accuracy threshold	100 units
Depth filtering	Disabled
Dense point cloud quality	High

conditions between the understory and overstory of the canopy, which could negatively impact photogrammetric reconstruction, we introduced luminance normalization before photogrammetry reconstruction, according to the findings by Kanellakis et al. (2020). Furthermore, to enhance operational feasibility, we automated scene orientation and scaling after the point cloud reconstruction process. Both additions are detailed below. All reconstruction and feature extraction steps were fully automated, except for tree delineation which, due to scene complexity, was performed manually. At the end of each reconstruction, the time it took to reconstruct each tree was recorded.

Video frames were extracted using FFMPEG (FFMPEG Team, France) at a rate of three FPS, balancing frame overlap with computational requirements per Olson et al. (2025). Frames were then subsequently luminance normalized (see Supplementary material). These frames were then photogrammetrically reconstructed into 3D models using the Python API for Metashape Professional Edition version 2.1.1 (Agisoft LLC, Russia). To do so, features were extracted from the imagery and used to align the images into a sparse point cloud. The sparse cloud was iteratively filtered, following recommendations by Over et al. (2021) and the Olson et al. (2025) workflow. Points with values exceeding 75% of the current mean value were removed until the predefined thresholds for each criterion were met (Table 1) or until the sequence limit was reached. The image count filter was excluded from this process to maintain long-range tie points and avoid overly aggressive filtering. Scenes were scaled and oriented (see below). To optimize computational demands for reconstruction, camera overlap was reduced to 10 cameras per point, using approximate meshes generated from low-resolution depth maps. Full resolution dense point clouds were then calculated and exported.

To scale and orient each scene during the reconstruction process, each face of the reference cube was automatically identified using its circular coded targets from the images before reconstruction. Distances were automatically defined between each face to constrain the reconstruction process. In cases where sufficient faces (3 or more) of the cube were not detected, an alternative approach was taken where the bole of each tree was aligned with the *z*-axis. Then, the tree was scaled according to the paper marker placed on the tree stem, as per Olson et al. (2025).

Point cloud pre-processing

To associate each point cloud with its corresponding ground-measurement data, the unique reference marker attached to each tree stem was matched across field notes, field video, and the reconstructed point clouds, using the unique sequential number assigned during field measurements. To reduce the influence of noise on subsequent analysis, the point clouds were filtered using Open3D (Zhou et al. 2018) and voxelated to a 1 cm^3 resolution (see Supplementary material). Ground points were classified using the Zhang et al. (2016) cloth simulation filter with a cloth resolution of 0.25 m and a class threshold of 0.1, implemented in the LidR package (Roussel et al. 2020) and R language and environment for statistical computing and graphics version 4.1.2 (R Core Team 2021). Heights were normalized, and any points below the identified ground plane were discarded.

Live-crown estimation

To estimate the crown base height (CBH), we implemented an automated histogram approach based on the vertical frequency distribution of live foliage across the height of the tree, as identified using the green-leaf index (GLI) (Louhaichi et al. 2001, Popescu and Zhao 2008, Olson et al. 2025), using the SciPy (Virtanen et al. 2020) and NumPy (Harris et al. 2020) Python Packages. The details of this process can be found in the Supplementary material.

Crown transparency

Crown transparency was calculated using a mechanistic ray-marching approach based on Olson et al. (2025), which approximates the direct (non-reflective) movement of 50 000 rays through the tree crown from a diffuse spherical ray-source surrounding the tree crown. Crown transparency was calculated as the proportion of ray energy passing through the canopy and the total number of rays, expressed as a dimensionless percentage ranging from 0 (fully opaque) to 100 (fully transparent). Ray energy was initialized at 1.0 and reduced by an attenuation factor (β) and dissipation constant (ς) on each valid collision with a canopy voxel. This approach was implemented using the Python programming language, NumPy, and the Numba compiler (Lam et al. 2015), and is outlined in full in the Supplementary material.

The parameters for the crown transparency model [voxel hit threshold (**N**), energy threshold (ε_t) attenuation factor (β), dissipation constant (ς)] was chosen through calibration against ground measurements using Bayesian optimization and 5-fold cross-validation. The optimization objective was defined as maximizing the negative of Huber's loss between the model output and all out-of-fold ground measurements. To assess how well the transparency model could generalize to out-of-sample data, the results of each cross-validation test were collected and used as the model transparency estimates.

DBH and height

Tree height was estimated from the voxelized point cloud by taking the 95th percentile for the height dimension. DBH was estimated using 3DFin (Laino et al. 2024).

Validation

To validate and assess the agreement of drone-based estimates, they were compared against field-estimated tree height, transparency, and DBH. For CBH, drone-based estimates were compared against estimates derived directly from the reconstructed point cloud by a trained

analyst, who identified crown-base height following two definitions. The first definition identified crown-base height as the location where foliage first appeared on the tree. The second definition, measured in cases where trees had clumps of foliage beneath the main canopy, established crown-base height as the location where sustained foliage first appeared, ignoring small clumps and branches with foliage disconnected from the larger crown.

The following metrics were calculated: Pearson's (r) and Spearman's (ρ) correlation coefficients to assess the strength of the relationship; Mean bias error (MBE) to quantify fixed bias, and root mean square error (RMSE) to quantify prediction error. To estimate the 95% confidence interval, the biased-corrected and accelerated (BCa) bootstrap method was used with 5000 resamples. Given the inherent subjectivity and potential for inter-observer bias in visual ground assessments (Solberg and Strand 1999, Redfern and Boswell 2004), lines of best fit were created using the OLS-Bisector method. Unlike standard linear regression, this method accounts for measurement error in both the dependent and independent variables (Saraçli and Türkan 2013).

Transparency estimate comparison

As the drone-based model captures the entire crown, including upper portions and occluded angles not visible to a ground observer, a direct comparison using a single, holistic transparency value is insufficient. To assess the influence of ray origin angle on drone-derived transparency and to determine which viewing angles most resemble ground-based visual assessments, ray-marched estimates were decomposed into distinct viewing strata. Estimates were grouped according to the position of their ray origins across 20-degree wide intervals, forming 162 viewing regions spherically distributed around the crown, with nine latitudinal and 18 longitudinal strata (Fig. 3). This stratified approach enables a more nuanced assessment into the effective perspective of a ground observer and quantifies how viewing angle and canopy structure impact transparency estimates. Further, because ground assessments were taken around each tree, the analysis of the horizontal strata provides an internal consistency check to confirm uniform modeling across the 360-degree azimuthal view.

The drone-derived estimates from each stratum were then compared with ground measurements using the metrics described in Section 2.5. Additionally, to quantify the internal consistency of the transparency estimates across strata, Cronbach's Alpha and Feldt's 95% confidence intervals were calculated (Feldt et al. 1987). Finally, because the assumptions for an analysis of variance (ANOVA) could not be reliably met due to sample size, the non-parametric Kruskal–Wallis H test, followed by a Dunn's post-hoc test, was used to identify significant differences between the median estimates of the strata.

Software and processing hardware

Photogrammetric reconstruction and tree attribute extraction were based on the workflow created in Olson et al. (2025), using the Python API for Metashape Professional Edition version 2.1.1 (Agisoft LLC, Russia), FFMPEG (FFMPEG Team, France), and ImageSharp (Six Labours, Australia). Point cloud delineation and crown live base truth-measurements were performed using CloudCompare, version 2.13 (CloudCompare Team 2024). Point clouds were normalized and cleaned to create digital terrain models (DTMs) using the LidR package (Roussel et al. 2020) and R Statistical Software, version 4.1.2 (R Core Team, 2021). DBH was estimated using 3DFin (Laino et al. 2024).

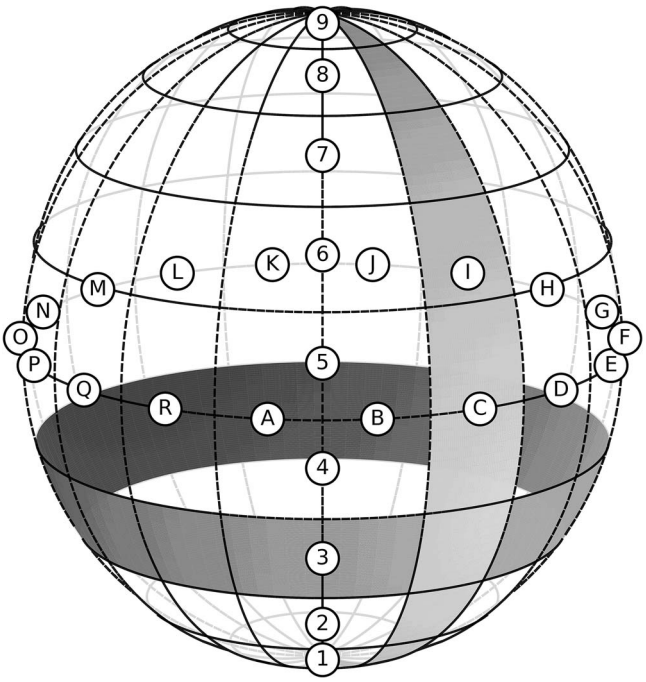

Figure 3 Illustration of the nine vertical (numbered) and 18 horizontal (lettered) strata across a unit sphere illustrating the bands of origin angles used to assess transparency with the ray-marching method. Vertical strata are formed between lines of latitude (highlighted in light gray), while the horizontal strata are formed between lines of longitude (highlighted in dark gray). Rays are evenly distributed across the sphere's surface.

Statistical analysis was performed using the SciPy Python Package (Virtanen et al. 2020). All statistical plots were created using Matplotlib (Hunter 2007). The map in Figure 2 was created using ArcGIS Pro (Esri 2025).

Processing was performed on a dedicated workstation running Windows 10 Enterprise Edition equipped with dual Intel Xeon Silver 4215R processors at 3193 MHz, dual NVIDIA Quadro RTX 4000 graphics processing units, and 128 GB of memory at 2400 MHZ. During processing, all files were stored on a dedicated Samsung 980 Pro NVMe SSD, with read and write speeds exceeding 5000 MB/s.

Results

During the reconstruction process, all but five ($n = 24$) trees had at least three faces of the reference cube detected, and all but one ($n = 28$) tree had at least two reference cube faces detected, allowing for the automated orientation of each scene. The remaining single tree was manually oriented and scaled. Qualitatively, all trees were successfully reconstructed with complete trunks and foliage.

Across the 29 flights, the mean video duration was 10.7 minutes (min/max: 4.4 minutes—15.7 minutes), with a standard deviation of 3.5 minutes. This corresponded to a mean automated reconstruction duration of ~652.4 minutes (min/max: 248.9 minutes—1287.8 minutes) per tree, with a standard deviation of 252.6 minutes.

The reconstructed trees in this study are generally well-defined, with most branches effectively captured (Fig. 4). Although the canopies tend to be visually fuzzy, the gaps appear well-defined within the crown. Branches and stems visible from outside the crown are mostly continuous, although there are a few disconnections along

Figure 4 Rendering of six photogrammetric reconstructed sugar maples from the sample set ($n = 29$). Point clouds have had terrain and surrounding vegetation removed for visualization purposes.

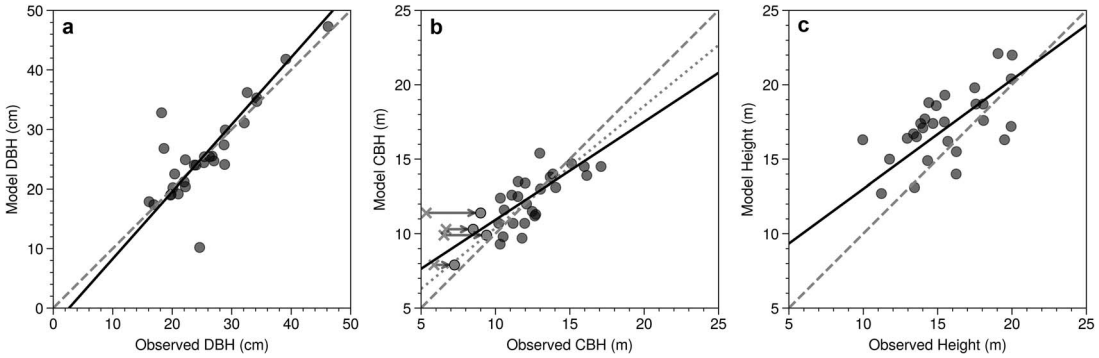

Figure 5 Dashed line represents perfect fit; solid line is the line of best fit. Each point is one tree. (a) Observed DBH vs. model-predicted DBH. (b) Manual point-cloud observed CBH vs. model-estimated CBH. X's show CBH values identified inclusive of sparse isolated foliage along the stem, while the arrows indicate their equivalent points identified exclusive of sparse isolated foliage. The sparsely and densely dashed lines represents perfect fit for the inclusion and exclusion definitions, respectively. (c) Ground-observed tree height vs. drone-based photogrammetry predicted tree height.

the longer limbs. While the reconstructed internal geometry of each crown appears well-defined at low to mid-height, the reconstruction quality decreases and becomes less well-defined in some trees, especially for fine twigs, near their tops.

DBH, height, and CBH

There is a strong correlation between the observed and model-predicted DBH (Fig. 5a; $r = 0.82$, 95% BCa CI [0.47, 0.96]; $\rho = 0.74$, BCa CI [0.31, 0.92]). Bias is not statistically significant (mbe = 0.27 cm, 95% BCa CI [−1.32 cm, 1.93 cm]). The majority of points remain close to the 1:1 line (cRMSE = 4.42 cm, 95% BCa CI [2.61 cm, 7.40 cm]); however, there is one significant outlier where the model DBH is significantly lower than the ground-observed DBH. The OLS-Bisector slope and intercept are minor and non-statistically significant, suggesting no significant proportional or fixed bias (slope = 1.13, 95% BCa CI [1.00, 1.44]; intercept = −2.99 cm, 95% BCa CI [−12.85 cm, 1.13 cm]).

Figure 5b illustrates the correlation between the point cloud-measured and model-estimated CBH. Four of the points are different between the two definitions (base of live-canopy vs. base of continuous live-canopy). For the first definition, there is a statistically significant moderate correlation ($r = 0.73$, 95% BCa CI [0.55, 0.86]) and Spearman's correlation ($\rho = 0.76$, BCa CI [0.55, 0.88]). Error is moderate (cRMSE = 1.94 m, 95% BCa CI [1.51 m, 2.76 m]) with low, non-statistically significant bias (mbe = 0.34 m, 95% BCa CI [−0.28 m, 1.14 m]). The OLS-Bisector analysis suggests the presence of proportional and fixed bias (slope = 0.66, 95% BCa CI [0.50, 0.85]; intercept = 4.35 m, 95% CI [1.83 m, 6.49 m]). When compared against CBH values identified using the second definition, the correlation is also significant and moderate ($r = 0.78$, 95% BCa CI [0.64, 0.89]; $\rho = 0.77$, 95% BCa CI [0.56, 0.89]). Moderate error is shown (cRMSE = 1.41 m, 95% BCa CI [1.19 m, 1.71 m]), with low, non-statistically significant bias (mbe = 0.01 m, 95% BCa CI [−0.49 m, 0.52 m]). The OLS-Bisector analysis suggests the presence of proportional bias but no fixed bias (slope = 0.82, 95% BCa CI [0.66, 1.03], and intercept = 2.2 m, 95% CI [−0.34 m, 4.27 m]).

There is a positive correlation between field-observed and drone-derived tree height (Fig. 5c; $r = 0.55$, 95% BCA CI [0.33, 0.74]; $\rho = 0.57$, 95% BCA CI [0.25, 0.78]) with moderate error (cRMSE = 2.71 m, 95% BCA CI [2.02 m, 3.98 m]) and statistically significant bias (mbe = 1.43 m, 95% BCA CI [0.26 m, 2.27 m]). While most predictions are higher than the ground-observed clinometer predictions, four trees are notably smaller. The OLS-Bisector analysis suggests the presence of proportional and fixed bias, showing a statistically significant slope of 0.73 (95% CI [0.47, 0.95]) and a statistically significant intercept of 6.90 m (95% CI [3.77, 10.37]).

Transparencies

Across all strata, the mean of the predictions from the ray-marching method is moderately correlated with estimations by ground-based observations ($r = 0.44$, 95% BCa CI [0.11, 0.66]; $\rho = 0.54$, 95% BCa CI

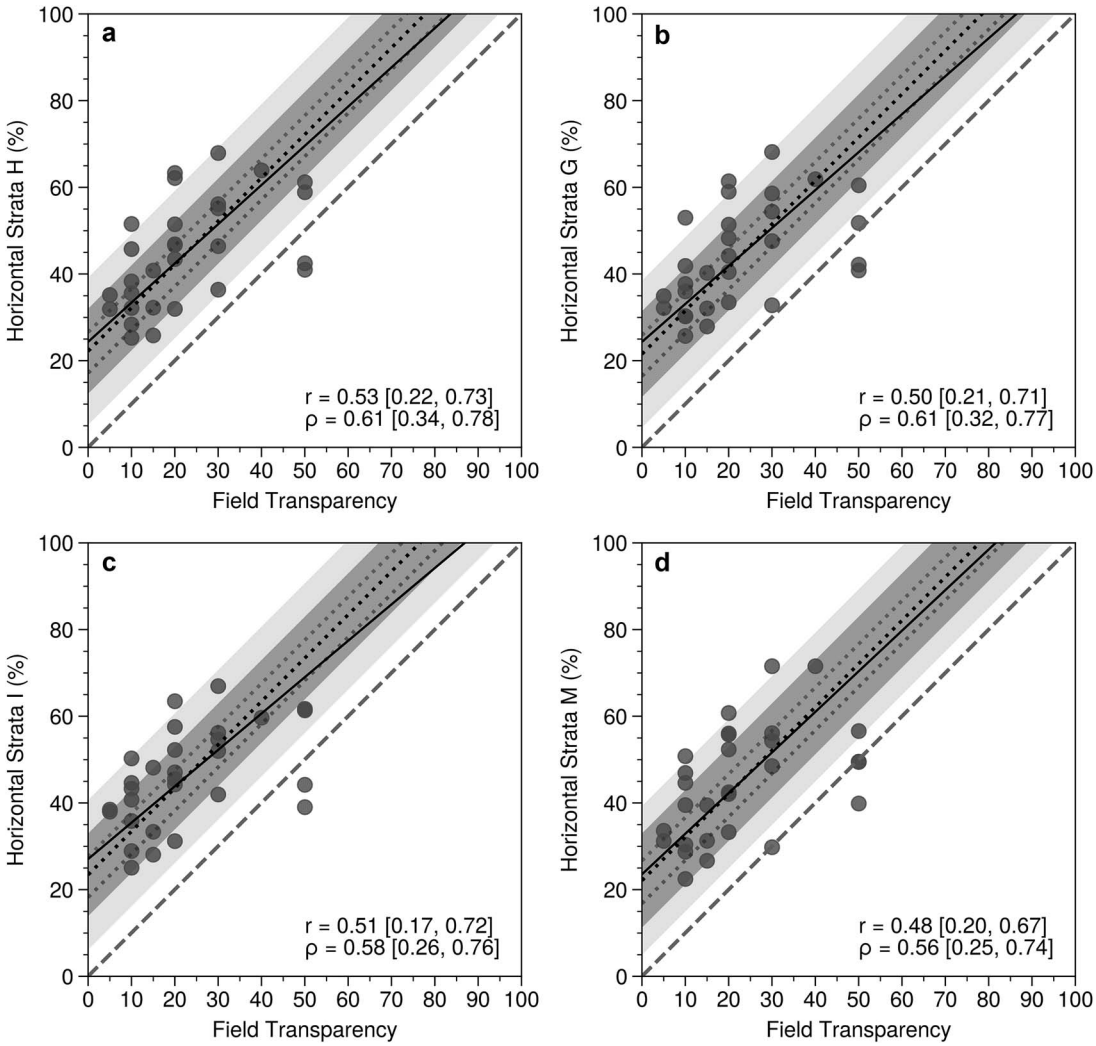

Figure 6 Comparisons of field-measured vs. model-estimated transparency for the top four horizontal strata, ranked by Spearman's correlation (a–d). Each plot displays the relationship between field transparency (%) and the corresponding model-estimated value for the given horizontal stratum. The solid black line represents the line of best fit between field transparency and the model transparency. The dashed gray line represents the 1:1 line of equality. The dotted black line represents the mean bias error, with the surrounding shaded gray areas representing the 95% confidence of the cRMSE. The darker shaded area represents the lower bound and the lighter area represents the upper bound. For each stratum, the Pearson correlation coefficient (r) and Spearman's correlation (ρ) are presented.

[0.25, 0.73]), but systematically overestimates (MBE = 21.66%, 95% BCa CI [16.10%, 26.12%]) with moderate random error (cRMSE = 13.79%, 95% BCa CI [10.68%, 17.93%]). There is a slight but non-significant OLS-Bisector slope (slope = 0.91, 95% BCa CI [0.70, 1.18]) and a statistically significant intercept (intercept = 23.80%, 95% CI [19.22%, 28.73%]), suggesting fixed bias but no proportional bias.

The correlation between observed and estimated crown transparency is similar across all horizontal strata, with stratum 'H' having slightly higher Spearman's ρ and Pearson's r values, while stratum 'B' has the lowest RMSE (Fig. 6). The Kruskal–Wallis H Test suggests no statistically significant differences between group medians for the horizontal strata ($H = 3.32$, $P = 1.00$). The 95% BCa CI for the OLS-Bisector Regression includes 1.0 for all strata, suggesting there is no significant proportional bias in any of the horizontal strata.

Across each of the nine vertical strata, ranging from 0 degrees to 180 degrees viewing angle, the second stratum (between 20 degrees and 40 degrees) has the highest Spearman correlation ($\rho = 0.59$, 95% BCa CI [0.33, 0.75]) between the single ground-observed crown transparency value and estimated crown transparency. The sixth stratum has the highest Pearson's correlation ($r = 0.52$, 95% BCa CI [0.30, 0.69]; Fig. 7). The eighth and ninth strata have no statistically significant correlation with ground values as their 95% BCa confidence intervals overlap zero across both Spearman and Pearson correlation values (see Supplementary material). Levene's test and the Shapiro–Wilk test suggest that the variances are equal and that the strata values are normally distributed. The Kruskal–Wallis H Test suggests a statistically significant difference between group means ($H = 68.77$, $P < .05$). The Dunn's post-hoc test suggests that there are no statistically significant differences among strata 1 through 7, nor a significant difference between strata 8 and 9; however, there are significant differences between the two groups. The 95% BCa CI for the OLS-Bisector Regression includes 1.0 for all strata, suggesting that there are no significant proportional biases in any of the vertical strata.

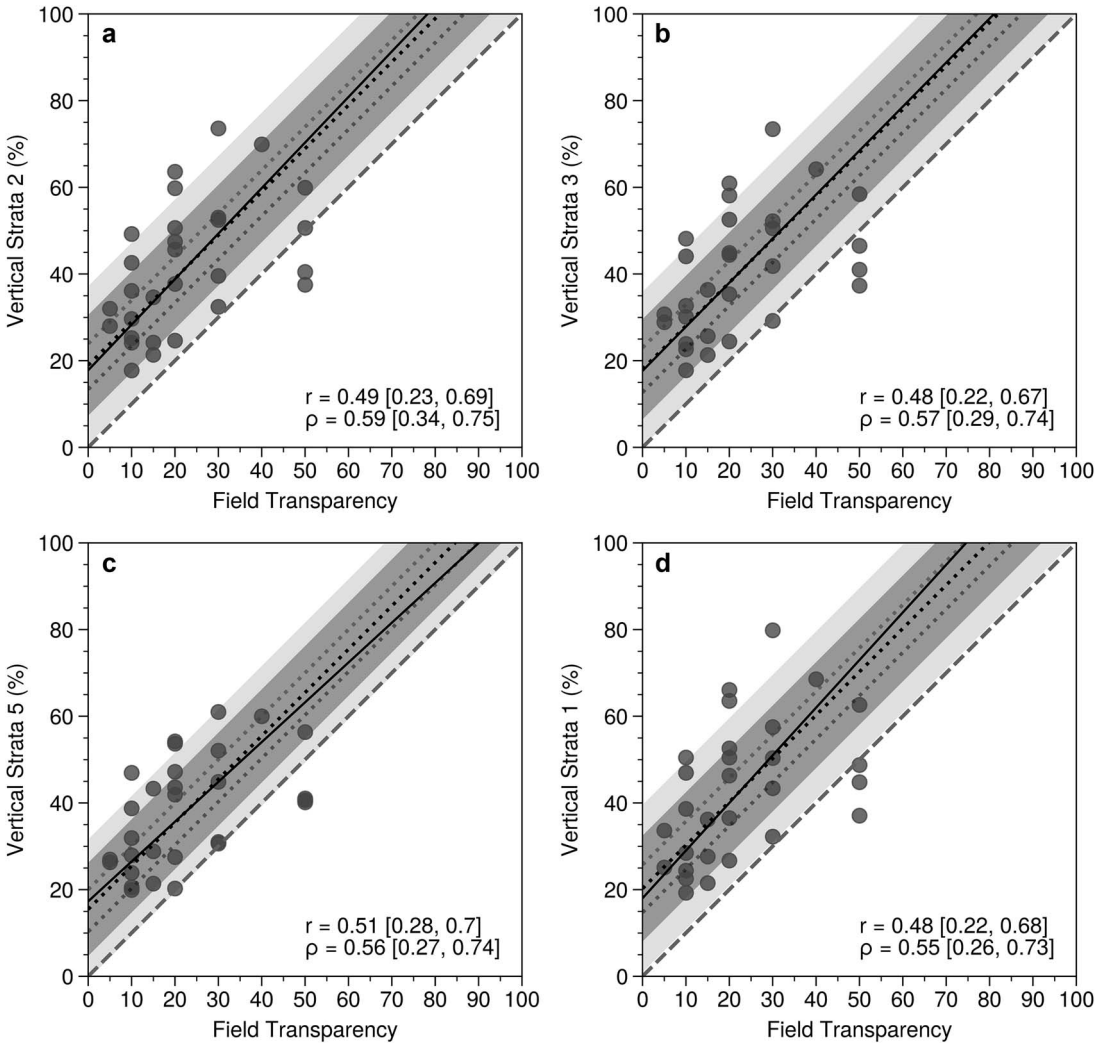

Figure 7 Comparisons of field-measured vs. model-estimated transparency for the top four vertical strata, ranked by Spearman's correlation (a–d). Each plot displays the relationship between field transparency (%) and the corresponding model-estimated value for the given vertical strata. The solid black line represents the line of best fit between field transparency and the model transparency. The dashed gray line represents the 1:1 line of equality. The dotted black line represents the mean bias error, with the surrounding shaded gray areas representing the 95% confidence of the cRMSE, with the darker shaded area representing the lower bound and the lighter area representing the upper bound. For each stratum, the Pearson correlation coefficient (r) and Spearman's correlation (ρ) are presented.

Transparency values for each tree remain consistent across the horizontal strata, with a mean transparency of ~41%. Higher field transparency estimations are generally predicted to have higher model transparency (Fig. 8a). The Cronbach's Alpha test for the horizontal strata yields a value of 1.00 (95% CI [0.99, 1.00]). Transparency error remains consistent, with less fluctuation in transparency values across the horizontal strata for trees with lower field transparency compared to those with higher field transparency (Fig. 8b). There is a mean error of ~20%. Trees with lower field transparency tend to have higher over-estimation (positive error), while trees with higher field transparency tend to have higher under-estimation (negative error).

Figure 8c shows the estimated transparency and error for each tree across the vertical strata. Values tend to decrease from strata 1 through 6 before rapidly increasing across strata 7 through 8 (Fig. 8c). This decrease appears to be more pronounced in trees with higher ground-assessed transparency, while the sharp increase is seen nearly universally across all sampled trees. Higher field transparency values generally correspond to higher model transparency values, with the latter showing less error than the former. Cronbach's Alpha test for the vertical strata yields a value of 0.98 (95% CI [0.97, 0.99]). Transparency error mirrors this pattern, with a moderate decrease between stratum 1 and 6, and a sharp increase in the trees with lower observed field transparency (Fig. 8d).

Discussion

The use of accurate and precise health assessments is crucial for making informed management decisions amidst unprecedented and intensifying forest disturbances. Within the northern hardwood forests, the repeat recommendations to predict vigor through crown condition further underscore the importance of an objective crown assessment to meet stand improvement targets. While the conventional ground-based approaches for evaluating crown transparency are well-established, their subjective nature, together with the lack of an applicable objective comparative standard, introduces challenges across spatio-temporal boundaries. Although the semi-automatic

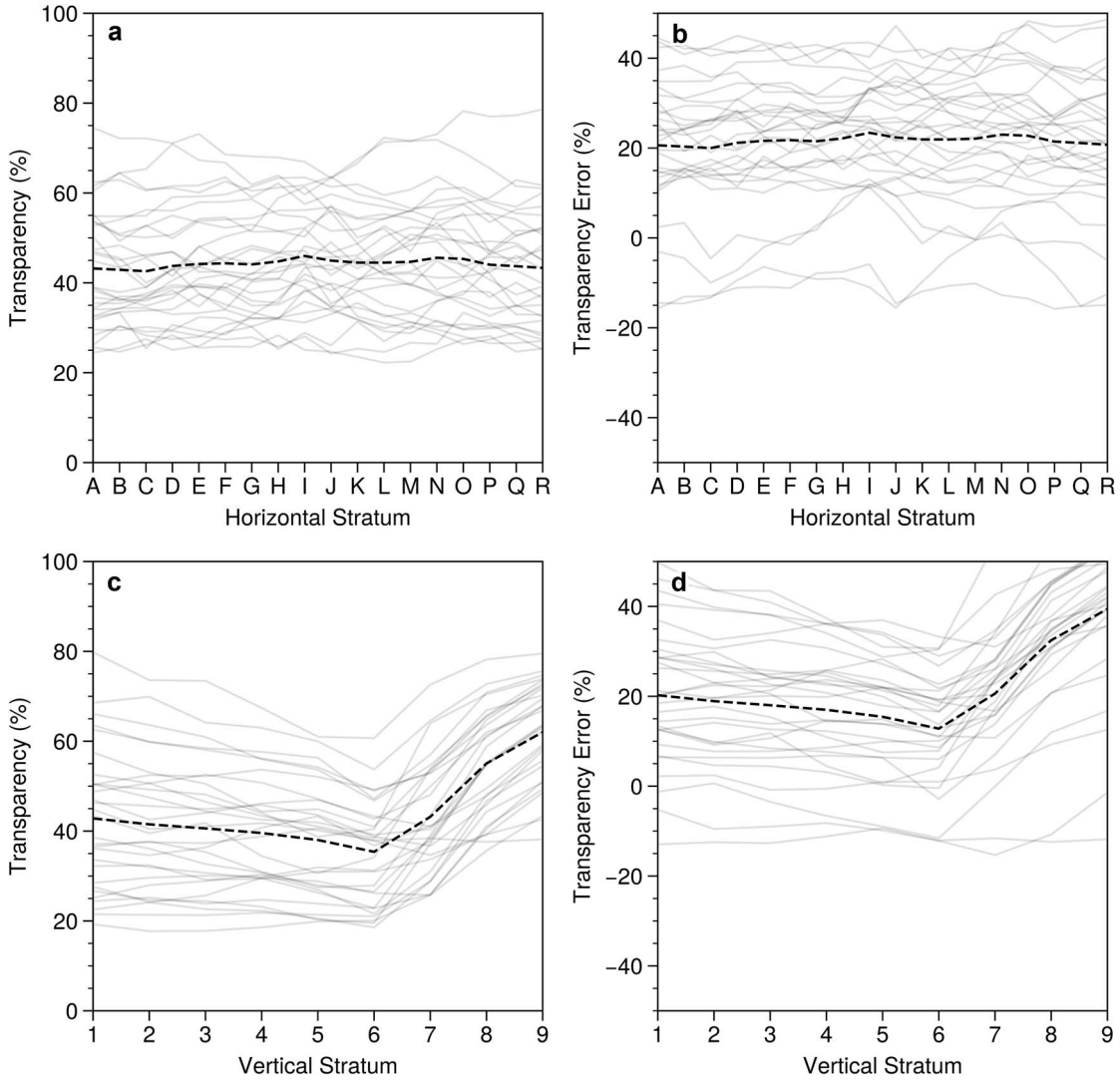

Figure 8 Spaghetti plots showing horizontal viewing strata, formed between evenly spaced longitudinal lines, vs. (a) predicted transparency, and (b) error against visual ground-assessments, and vertical stratums formed between evenly spaced latitudinal lines, vs. (c) predicted transparency, and (d) error against visual ground-assessments. The black dashed line represents the mean value across all 29 trees. Each gray line represents an individual tree.

analyses of 2D images (e.g., CROCO, ForestCrowns) are valuable calibration standards for improving the objectivity of ground-based observations, their wider application remains limited within denser forest stands where poor visual contrast often exists between the subject tree and its background.

This foundational exploratory study investigates intra-canopy drone photogrammetry as a complementary three-dimensional approach, generating tree-scale reconstructions from video imagery captured from beneath, within, and above the forest canopy. Although the results from this study cannot be extrapolated beyond the dataset of 29 trees, the methodological developments and results successfully demonstrate initial viability, expanding prior work from open-grown urban settings (Olson et al. 2025, $n = 19$, 2× replicates under leaf-off and leaf-on conditions) into more complex, natural systems. The analytical ray-marching approach used in this study to predict crown transparency demonstrates the influence of ray incident angle on agreement and disagreement, shows that crown observation angle may influence crown transparency values, and establishes a potential quantitative spatial assessment for crown transparency against which conventional ground-based assessments can be compared and calibrated.

Agreement, precision, and bias of structural attribute estimates

The results support previous findings that the drone-based methodology can provide an effective approach for estimating DBH. The strong correlation and low bias for DBH estimates ($r = 0.82$, cRMSE = 4.42 cm, mbe = 0.27 cm) are attributable to both the robustness of the 3DFin model and the inherent reliability of the field-based DBH tape measurements, and are comparable to the 3DFin photogrammetry benchmark (RMSE = 3.96 cm) reported by Laino et al. (2024), but are weaker than results shown under open-grown urban conditions by ∼1 cm ($r = 0.93$, RMSE = 2.90 cm) (Olson et al. 2025).

There was strong correlation between the automated histogram CBH estimates and manual point-cloud observations. Still, one

potential source of disagreement arose from the human interpreter's inclusion of small, isolated foliage clusters as the start of the live crown, present in four trees but which the histogram approach explicitly excludes. When comparing histogram values against the secondary definition of crown-base height, consistent improvement is shown across error, correlation, and slope. It reduced the RMSE by 0.57 m (from 1.98 m to 1.41 m) and effectively eliminated the positive bias seen on these samples, reducing Mean Bias Error (MBE) from 0.34 m to 0.01 m. Correlation also increased ($r = 0.73$, $\rho = 0.76$ vs. $r = 0.78$, $\rho = 0.77$). The histogram approach was explicitly designed to ignore isolated foliage because understory foliage can disproportionately increase the volume of the crown convex hull relative to its contribution to the tree's total photosynthetic capacity. While it is expected that the bias in transparency values would increase if the histogram approach were modified to search for the first definition, its significance in the larger population is unknown with the small dataset size in this study. Future work should explore how these definition differences may impact the overall transparency values, and the benefits of using one over the other in terms of implications for further health assessment modeling.

While similar in terms of random error to CBH, tree height estimations demonstrated much greater fixed bias and weaker correlation. The agreement of tree height estimation is notably lower than in previous studies, with the centered RMSE (cRMSE) being nearly double the uncentered RMSE found in urban trees (2.71 m vs. 1.54 m) (Olson et al. 2025). Further, the difference in mean bias error in tree height (1.43 m) and crown-base height (0.34 m; 0.01 m) indicates that error can be partially explained by challenges identifying the terminal leader of the trees during ground observations using the clinometer method (Martin 2022). Identifying the absolute highest point of a broad, dense sugar maple crown from the ground is challenging due to forking stems and poor visibility. The presence of proportional bias, as identified by the OLS-Bisector slopes in the estimation of both CBH and height, is introduced by the presence of overestimations in lower CBH and height ranges. Secondary sources of error are attributable to noise in the point cloud caused by branch movement between frames and poor spectral detail during feature matching. Near the top of the crowns, spectral detail is qualitatively degraded by oversaturated luminance levels introduced during the transition from a dark understory to a bright sky. While partially corrected through luminance normalization, noise from the fine branches of the terminal leader is amplified in some trees. This contrasts with the strong performance of the DBH estimates, derived from the lower bole—a geometrically simpler, more stable, and better-textured part of the tree model less affected by lighting fluctuations and scene movement.

Transparency

When comparing mean crown transparency with previous work in open-grown urban environments, this study found weaker correlation and greater fixed bias. Despite this, the centered RMSE was found to be similar to the uncentered RMSE calculated under urban environments (13.79% vs. 12.61%), suggesting that the fundamental agreement of the ray-marching method likely remains robust when transitioning to more complex forest structures, provided that this fixed bias (mbe = 21.66%) can be addressed through calibration. The more pronounced bias in this study might be attributable to a conceptual mismatch between the model and human perception in larger trees.

The ray-marching approach quantifies volumetric porosity across a crown volume defined by a convex hull, which, for the irregular crowns of sugar maples, includes large volumes where foliage is not physiologically expected. This bias is compounded by the inherent subjectivity of ground-truth data, with known inter-observer variability ranging between 5% and 10% (Solberg and Strand 1999, Redfern and Boswell 2004). Because of this, the ray-marched transparency metrics in this study is better conceptually understood as a distinct yet highly related objective measure of crown density. This new metric provides value as an objective and likely more accurate measurement of crown density, which could be used as indicator of photosynthesis potential and in models of the overall vigor of a given tree. Further work should explore with a larger dataset the relationship of this new metric against other physiological vigor indicators like including dieback or annual diameter growth. With a much larger and diverse dataset involving a wider range of forest conditions and ground-assessors, these values could model the average conventional authoritative ground-assessed transparency and could be used to calibrate ground assessors across large spatial extents.

To determine which viewing angles produced estimates most analogous to ground-based visual assessments, the model-derived transparency metric was decomposed by vertical and horizontal strata. The results show that transparency estimates are strongly vertically anisotropic but are horizontally isotropic; while no statistically significant differences in median transparency were found among the horizontal strata, significant differences among vertical strata divided them into two distinct groups (strata 1–7 and 8–9). The strongest correlation with ground measurements was observed within the lower crown, a stronger relationship than that of the complete crown. Conversely, the upper viewing strata showed no statistically significant correlation with ground observations, indicating that a ground observer's effective perspective is biased toward the lower portions of the crown, and that the upper crown when viewed from the ground are effectively occluded or misinterpreted as belonging to another tree. Given that dieback in sugar maple typically begins within the upper canopy and progresses downward, this finding implies that ground assessments may fail to detect early signs of decline that are occluded by denser, mid-canopy foliage, albeit a larger sample size is required to generalize this conclusion. Despite this apparent anisotropy, the high Cronbach's Alpha scores for the vertical and horizontal strata suggest there is strong internal consistency in each reconstructed tree, supporting the decomposition of the metric into individual strata.

Sources and influence of error

Several interactions across the drone video capture, reconstruction, and point cloud analysis processes influenced the final precision and agreement of the structural attributes. During drone video capture, two significant sources included the extreme contrast between the dark understory and the bright sky, and the complex shading environment, both of which were compounded by branch movement between video frames. Movement across frames, when combined with a high input frame count in the photogrammetry process, resulted in finer branches being erroneously matched multiple times in slightly different spots during gusts of strong wind, leading to point duplication (noise) in the upper crown. Another environmental factor impacting the upper crown, light, introduced oversaturation in the camera and reduced RGB information at the top of the canopy in

captures taken midday, causing many points in the upper crown to be pure white. While luminance normalization was introduced to reduce the impact of lighting conditions, the cameras' dynamic range was insufficient to maintain consistent imaging without clipping, and information was lost at capture.

The impact of these duplicate points and discoloration varied widely across metrics. For example, the DBH estimates remained highly accurate because of minimal influence from changing lighting conditions or movement across the lower stem; in contrast, the upper crown was significantly noisier in the final 2–3 meters, potentially hindering accurate identification of the tree's highest point. When interpreted considering the difficulty in accurately identifying leaders during ground assessments, this may explain the observed bias in tree height, and the increased error compared to more straightforward urban environments. Similarly, branch movement may have increased the calculated crown density estimates by introducing duplicate voxels, while discoloration may have had the opposite impact through filtering. Qualitative observation of the voxelated point clouds during processing suggests that both error sources were partially mitigated by the voxelation process and by the minimum-hit criteria during ray-marching. Further experimentation using synthetic tree point clouds may be warranted in future studies.

The ray-marching metric's high internal consistency suggests that noise does not introduce catastrophic interference in the trees studied or significantly alter how crown density is perceived from different angles. This makes it potentially viable to address the large systemic offset (MBE = 21.66%) in transparency assessments and to align this measure with conventional methods using a linear transformation. The result would be a transparency estimate normalized to the average field-based assessment, provided a sufficiently large dataset. This standardized metric can be used to train and calibrate human assessors and mitigate inter-observer variability. Further, while all parameters were carefully chosen according to conservative defaults originating in the literature, the interactions across reconstruction, denoising, and analysis parameters for crown-base height, transparency, and height percentile may also impact the final estimates. While much beyond the scope of this exploratory work, industrial applications may benefit from a large-scale sensitivity analysis and optimization to adapt better to the characteristics of a given drone flight (vibrations, speed, distance from tree), forest type, canopy density, and lighting conditions.

Scalability

The real-world adoption and application of drone-based photogrammetry for the reconstruction of individual trees under industrial contexts demand that this methods in tree-level mensuration provide enhanced insights into the attributes of the tree, increase the accuracy or objectivity of estimates, and can do so more efficiently than conventional approaches. The method, as presented, suggest the capacity to offer greater resolution and objectivity when estimating attributes not directly measurable from the ground, like transparency. However, its wider adoption outside of academia or as a comparative quantitative standard remains restricted by poor field efficiency and high cost of trained drone pilots. For this reason, we do not argue that this method is a universal viable replacement for current ground-based visual approaches. However, we do argue that the strength of this approache comes from its apparent ability to provide a high-resolution, objective snapshots of individual trees. Future work should explore the potential to improve efficiency and reduce costs associated with captures, as well as to explore a wider variety of crown metrics that could be associated with tree health.

Current efficiency for the baseline approach is outlined in Olson et al. (2025), finding that the average tree reconstruction took on average, ∼4 hours per tree under urban conditions and a mean footage duration of ∼4 minutes. In this paper, the average footage duration was around double at 10.7 minutes. This corresponded to a much greater mean processing duration of 652.4 minutes (∼11 hours) per tree, with 20 additional minutes allocated to delineating each tree from its surroundings. Time spent validating point clouds had minimal impact, taking <5 minutes of manual processing per reconstruction. Individual drone flights were limited by battery capacity, daylight availability, traveling to and from the sites, and pilot fatigue.

Future technological developments to increase cost-effectiveness and efficiency include the development of algorithms to automatically delineate individual trees under natural forest conditions, and autonomous drone piloting to navigate and acquire video imagery without human assistance. While current approaches for photogrammetric reconstruction are reliable, overall processing efficiency, like scene scaling, might be improved through end-to-end deep learning models or by leveraging in-flight extrinsic parameters extracted from the drone and the environment, including barometric readings or real-time kinematics (RTK).

Limitations and future work

While this study demonstrates a promising approach for assessing crown condition, the findings are constrained by several factors, including its small sample size of 29 trees and the qualitative nature of ground-based transparency measures. Furthermore, significant technical barriers may hinder the operational deployment of this methodology in higher-density, unmanaged stands. The most critical of these include texture loss from poor lighting and foliage occlusion, followed by challenges with automated crown delineation and the difficulty of maneuvering the drone beneath the canopy during imagery acquisition.

For photogrammetric reconstruction, the extreme dynamic range between the heavily shaded sub-canopy and brightly lit super-canopy creates a significant challenge during feature matching. While this study addressed this issue through luminance normalization, an approach which can enhance reconstruction in low-light environments like underground tunnels (Kanellakis et al. 2020), this process can amplify noise. Future applications would benefit from employing higher-quality cameras with high-dynamic range (HDR) support to avoid luminance compression errors.

Widescale application is also constrained by the reliance on manual tree delineation, a process that becomes subjective and tedious when there are many canopies in proximity. Although this was not a significant issue for the relatively dominant trees in this study, it could become problematic when assessing larger datasets. The operationalization of this method demands exploring automated tree-level segmentation approaches, like skeletonization (Dobbs et al. 2024, Li et al. 2024, Yang et al. 2024). In operational applications, the data acquisition process itself introduces further limitations. The skills required to navigate the drone around occluding branches necessitate the development of automated flight routines. During acquisition, inadequate video coverage from occluding tree geometry can lead to incomplete reconstructions. Similarly, understory vegetation can

obscure the reference cube used for scaling and orientation. Of the 29 reconstructed scenes, five could not be automatically scaled or oriented because of occluded fiducial patterns on the reference cube. This could be mitigated by clearing the area around the tree stem, elevating the fiducial cube on a stand, or implementing a post-reconstruction spatialized fiducial detection pass that locates known points according to the textured 3D geometry rather than relying solely on the original 2D images.

Finally, the transparency model itself could be refined. A primary challenge is to explore whether an alternative voxel-based concave hull could provide a more ecologically accurate representation of the crown than the current convex hull (Borianne et al. 2017), which does not exclude large, non-foliated gaps between major branches. Such validation could be achieved by correlating the derived crown volume against direct biophysical measurements, such as a destructively sampled leaf area or biomass. Future work should also move beyond transparency to derive other health indicators from the point clouds, including crown dieback, which will require addressing the classification challenge of automatically delineating leafless branches from natural canopy gaps, enabling further work toward developing normalized metrics not currently viable from ground-based assessments, such as transparency estimates corrected for the volumetric influence of large crowns (Metzger and Oren 2001). Finally, the identified vertical anisotropy warrants consideration and exploration in future studies to confirm that it is physiologically present in the trees studied. Similar decomposition should be considered in future studies when comparing transparency estimates to ground estimates, and caution should be taken when interpreting above-canopy remote sensing data as a direct proxy for conventional, ground-based metrics of crown condition.

Conclusion

This study demonstrates the feasibility of using intra-canopy drone photogrammetry for detailed 3D modeling and the estimation of health attributes of sugar maple trees in moderate-density northern hardwood forests. The methodology presents an approach for estimating CBH and supports the 3DFin tool for DBH estimation from photogrammetric point clouds. While the ray-marching approach delivers internally consistent measurements of crown transparency, the moderate correlation with subjective ground-based assessments highlights inherent inconsistencies. Further research is required to address questions surrounding point-cloud reliability and variance, as the relationship between the estimates and true transparency values remains unknown. This study highlights the potential for drone-based intra-canopy photogrammetry to serve as an objective assessment at the individual tree level, providing a more nuanced and accurate tool for understanding tree-level health.

Acknowledgements

The authors would like to thank Dr David Voyer, Emmanuelle Baby-Bouchard, and all those who supported and provided advice during the fieldwork and analysis associated with this paper.

Author contributions

Lukas G. Olson (Conceptualization, Data curation, Formal analysis, Investigation, Methodology, Software, Validation, Visualization, Writing—original draft, Writing—review & editing), Nicholas C. Coops (Conceptualization, Funding acquisition, Investigation, Project administration, Resources, Supervision, Writing—review & editing), Guillaume Moreau (Conceptualization, Writing—review & editing), Richard C. Hamelin (Conceptualization, Writing—review & editing), and Alexis Achim (Conceptualization, Funding acquisition, Writing—review & editing)

Supplementary material

Supplementary material are available at *Forestry* online.

Conflict of interest

The authors declare that they have no known competing financial interests or personal relationships that could have appeared to influence the work reported in this paper.

Funding

This research was supported by the Natural Sciences and Engineering Research Council of Canada (NSERC) Alliance project Silva21 (Grant Number ALLRP 556265–20). grantee Prof. Alexis Achim.

Data availability

Data will be available upon request. The GitHub repository associated with the workflow will be updated upon publication to include the developments made in this study.

References

Arkin J, Coops NC, Daniels LD *et al.* Estimation of vertical fuel layers in tree crowns using high density LiDAR data. *Remote Sens* 2021;**13**:4598.

Bishop DA, Beier CM, Pederson N *et al.* Regional growth decline of sugar maple (Acer saccharum) and its potential causes. *Ecosphere* 2015;**6**:1–14. https://doi.org/10.1890/ES15-00260.1.

Borianne P, Subsol G, Caraglio Y. Automated efficient computation of crown transparency from tree silhouette images. *Comput Electron Agric* 2017;**133**:108–18.

Caputo J, Beier CM, Sullivan TJ *et al.* Modeled effects of soil acidification on long-term ecological and economic outcomes for managed forests in the Adirondack region (USA). *Sci Total Environ* 2016;**565**:401–11. https://doi.org/10.1016/j.scitotenv.2016.04.008.

Cherubini P, Battipaglia G, Innes JL. Tree vitality and forest health: can tree-ring stable isotopes be used as indicators? *Curr For Rep* 2021;**7**:69–80. https://doi.org/10.1007/s40725-021-00137-8.

Chisholm RA, Cui J, Lum SKY *et al.* UAV LiDAR for below-canopy forest surveys. *J Unmanned Veh Syst* 2013;**01**:61–8.

Chisholm RA, Rodríguez-Ronderos ME, Lin F. Estimating tree diameters from an autonomous below-canopy UAV with mounted LiDAR. *Remote Sens* 2021;**13**:2576.

Cleavitt NL, Battles JJ, Johnson CE *et al.* Long-term decline of sugar maple following forest harvest, Hubbard brook experimental forest. *New Hampshire Can J For Res* 2018;**48**:23–31.

CloudCompare Team. CloudCompare. http://www.cloudcompare.org/ (29 January 2024, date last accessed).

Dobbs H, Batchelor O, Peat C *et al.* Quantifying robustness: 3D tree point cloud skeletonization with smart-tree in noisy domains. *Pattern Anal Appl* 2024;**27**:28. https://doi.org/10.1007/s10044-024-01238-3.

Ecke S, Dempewolf J, Frey J *et al.* UAV-based forest health monitoring: a systematic review. *Remote Sens* 2022;**14**:3205.

Ecke S, Stehr F, Frey J *et al.* Towards operational UAV-based forest health monitoring: species identification and crown condition assessment by means of deep learning. *Comput Electron Agric* 2024;**219**:108785.

Environment and Climate Change Canada. Canadian Climate Normals 1991-2020 Station Data for Thetford Mines. 2025. Available from: https://climate.weather.gc.ca/climate_normals/results_1961_1990_e.html?searchType=stnProx&txtRadius=25&optProxType=station&coordsStn=45.966667|-71.6|ST+FORTUNAT&txtCentralLatMin=0&txtCentralLatSec=0&txtCentralLongMin=0&txtCentralLongSec=0&stnID=1331&dispBack=0.

Esri. World Imagery [dataset]. *ArcGIS Living Atlas of the World* 2024. https://services.arcgisonline.com/ArcGIS/rest/services/World_Imagery/MapServer.

Esri. *ArcGIS Pro (Version 3.5.1) [Software]*. Redlands, CA: Environmental Systems Research Institute, 2025. https://www.esri.com/en-us/arcgis/products/arcgis-pro/overview.

Feldt LS, Woodruff DJ, Salih FA. Statistical inference for coefficient alpha. *Appl Psychol Measur* 1987;**11**:93–103.

Ferretti M. Forest health assessment and monitoring—issues for consideration. *Environ Monit Assess* 1997;**48**:45–72.

Frampton C, Pekelharing C, Payton I. A fast method for monitoring foliage density in single lower-canopy trees. *Environ Monit Assess* 2002;**72**:227–34.

Gatziolis D, Lienard JF, Vogs A *et al.* 3D tree dimensionality assessment using photogrammetry and small unmanned aerial vehicles. *PloS One* 2015;**10**:e0137765. https://doi.org/10.1371/journal.pone.0137765.

Gbondo-Tugbawa SS, Driscoll CT, Mitchell MJ *et al.* A model to simulate the response of a northern hardwood forest ecosystem to changes in S deposition. *Ecol Appl* 2002;**12**:8–23.

Giannetti F, Puletti N, Quatrini V *et al.* Integrating terrestrial and airborne laser scanning for the assessment of single-tree attributes in Mediterranean forest stands. *Eur J Remote Sens* 2018;**51**:795–807.

Goodbody TRH, Coops NC, Hermosilla T *et al.* Digital aerial photogrammetry for assessing cumulative spruce budworm defoliation and enhancing forest inventories at a landscape-level. *ISPRS J Photogramm Remote Sens* 2018;**142**:1–11.

Goodbody TRH, Coops NC, White JC. Digital aerial photogrammetry for updating area-based Forest inventories: a review of opportunities, challenges, and future directions. *Curr For Rep* 2019;**5**:55–75.

Harris CR, Millman KJ, van der Walt SJ *et al.* Array programming with NumPy. *Nature* 2020;**585**:357–62. https://doi.org/10.1038/s41586-020-2649-2.

Hunter JD. Matplotlib: a 2D graphics environment. *Comput Sci Eng* 2007;**9**:90–5.

Kanellakis C, Karvelis P, Nikolakopoulos G. On image based enhancement for 3D dense reconstruction of low light aerial visual inspected environments. In: Arai K, Kapoor S, (eds.). *Advances in Computer Vision*. Cham: Springer International Publishing, 2020, 265–79.

Laino D, Cabo C, Prendes C *et al.* 3DFin: a software for automated 3D forest inventories from terrestrial point clouds. *For Int J For Res* 2024;**97**:479–96.

Lam SK, Pitrou A, Seibert S. *Numba: A LLVM-Based Python JIT Compiler. Proceedings of the Second Workshop on the LLVM Compiler Infrastructure in HPC*. New York, NY, USA: Association for Computing Machinery, 2015, 1–6.

Lee AC, Lucas RM. A LiDAR-derived canopy density model for tree stem and crown mapping in Australian forests. *Remote Sens Environ* 2007;**111**:493–518.

Li X, Liu B, Shi Y *et al.* Efficient three-dimensional reconstruction and skeleton extraction for intelligent pruning of fruit trees. *Comput Electron Agric* 2024;**227**:109554.

Louhaichi M, Borman MM, Johnson DE. Spatially located platform and aerial photography for documentation of grazing impacts on wheat. *Geocarto Int* 2001;**16**:65–70.

Martin AJF. Accuracy and precision in urban forestry tools for estimating total tree height. *Arboric Urban For AUF* 2022;**48**:319–32.

Metzger JM, Oren R. The effect of crown dimensions on transparency and the assessment of tree health. *Ecol Appl* 2001;**11**:1634–40.

Miller J, Morgenroth J, Gomez C. 3D modelling of individual trees using a handheld camera: accuracy of height, diameter and volume estimates. *Urban For Urban Green* 2015;**14**:932–40.

Mizoue N, Dobbertin M. Detecting differences in crown transparency assessments between countries using the image analysis system Croco. *Environ Monit Assess* 2003;**89**:179–95.

Moreau G, Achim A, Pothier D. Relevance of stem and crown defects to estimate tree vigour in northern hardwood forests. *For Int J For Res* 2020a;**93**:630–40. https://doi.org/10.1093/forestry/cpaa005.

Moreau G, Cecil-Cockwell MJL, Pothier D *et al.* Visual assessment of tree vigour in Canadian northern hardwood forests: the need for a simplified system. *For Ecol Manage* 2023a;**529**:120720. https://doi.org/10.1016/j.foreco.2022.120720.

Moreau G, Chagnon C, Cecil-Cockwell MJL *et al.* Simplified tree marking guidelines enhance value recovery as well as stand vigour in northern hardwood forests under selection management. *For Int J For Res* 2023b;**97**:183–93. https://doi.org/10.1093/forestry/cpad045.

Morin RS, Randolph KC, Steinman J. Mortality rates associated with crown health for eastern forest tree species. *Environ Monit Assess* 2015;**187**:1–11.

Olson LG, Coops NC, Moreau G *et al.* The assessment of individual tree canopies using drone-based intra-canopy photogrammetry. *Comput Electron Agric* 2025;**234**:110200.

Oswald EM, Pontius J, Rayback SA *et al.* The complex relationship between climate and sugar maple health: climate change implications in Vermont for a key northern hardwood species. *For Ecol Manage* 2018;**422**:303–12.

Ouimet R, Moore J-D, Duchesne L. Soil thresholds update for diagnosing foliar calcium, potassium, or phosphorus deficiency of sugar maple. *Commun Soil Sci Plant Anal* 2013;**44**:2408–27.

Over J-SR, Ritchie AC, Kranenburg CJ *et al. Processing Coastal Imagery with Agisoft Metashape Professional Edition, Version 1.6—Structure from Motion Workflow Documentation*. Reston, VA: U.S. Geological Survey, 2021.

Popescu SC, Zhao K. A voxel-based lidar method for estimating crown base height for deciduous and pine trees. *Remote Sens Environ* 2008;**112**:767–81.

Pothier D, Fortin M, Auty D *et al.* Improving tree selection for partial cutting through joint probability modelling of tree vigor and quality. *Can J For Res* 2013;**43**:288–98.

R Core Team. *R: A Language and Environment for Statistical Computing*. Vienna, Austria: R Foundation for Statistical Computing, 2021.

Randolph KC. Development history and bibliography of the US Forest Service crown-condition indicator for forest health monitoring. *Environ Monit Assess* 2013;**185**:4977–93. https://doi.org/10.1007/s10661-012-2919-z.

Randolph KC, Morin RS, Steinman J. *Descriptive Statistics of Tree Crown Condition in the Northeastern United States. Asheville, NC*: U.S. Department of Agriculture, Forest Service, Southern Research Station, 2010, (General Technical Report SRS-GTR-124).

Randolph KDC. *Forest Health Monitoring: 2006 National Technical Report Chapter 8. Asheville, NC*: U.S. Department of Agriculture, Forest Service, 2006, 65–109.

Redfern DB, Boswell RC. Assessment of crown condition in forest trees: comparison of methods, sources of variation and observer bias. *For Ecol Manage* 2004;**188**:149–60.

Roberts JW, Koeser AK, Abd-Elrahman AH *et al.* Terrestrial photogrammetric stem mensuration for street trees. *Urban For Urban Green* 2018;**35**:66–71.

Roussel J-R, Auty D, Coops NC *et al.* lidR: an R package for analysis of airborne laser scanning (ALS) data. *Remote Sens Environ* 2020;**251**:112061.

Saraçli S, Türkan AH. A comparison of linear regression techniques in method comparison studies. *J Stat Comput Simul* 2013;**83**:1890–9.

Scher CL, Griffoul E, Cannon CH. Drone-based photogrammetry for the construction of high-resolution models of individual trees. *Trees* 2019;**33**:1385–97.

Schomaker ME, Zarnoch SJ, Bechtold WA *et al. Crown-Condition Classification: A Guide to Data Collection and Analysis*. Asheville, NC: U.S. Department of Agriculture, Forest Service, Southern Research Station, 2007, SRS-GTR-102.

Solberg S, Strand L. Crown density assessments, control surveys and reproducibility. *Environ Monit Assess* 1999;**56**:75–86.

Tominaga K, Watmough SA, Aherne J. Predicting tree survival in Ontario sugar maple (Acer saccharum) forests based on crown condition. *Can J For Res* 2008;**38**:1730–41.

Virtanen P, Gommers R, Oliphant TE *et al.* SciPy 1.0: fundamental algorithms for scientific computing in python. *Nat Methods* 2020;**17**:261–72. https://doi.org/10.1038/s41592-019-0686-2.

de Vries W, Vel E, Reinds GJ *et al.* Intensive monitoring of forest ecosystems in Europe: 1. Objectives, set-up and evaluation strategy. *For Ecol Manage* 2003;**174**:77–95.

Yang Y, Lai H, Chen B *et al.* Automatic method for extracting tree branching structures from a single RGB image. *Forests* 2024;**15**:1659.

Zarnoch SJ, Bechtold WA, Stolte KW. Using crown condition variables as indicators of forest health. *Can J For Res* 2004;**34**:1057–70.

Zhang W, Gao F, Jiang N *et al.* High-temporal-resolution Forest growth monitoring based on segmented 3D canopy surface from UAV aerial photogrammetry. *Drones* 2022;**6**:158.

Zhang W, Qi J, Wan P *et al.* An easy-to-use airborne LiDAR data filtering method based on cloth simulation. *Remote Sens* 2016;**8**:501.

Zhou Q-Y, Park J, Koltun V. *Open3D: A Modern Library for 3D Data Processing*. Ithaca, NY: arXiv, 2018. https://arxiv.org/abs/1801.09847v1 (December 2, 2025, date last accessed).

Zhu Z, Kleinn C, Nölke N. Assessing tree crown volume—a review. *For Int J For Res* 2021;**94**:18–35.

Forestry: An International Journal of Forest Research, 2026, **99**, cpag006
https://doi.org/10.1093/forestry/cpag006
Original Article